Journal of Biomolecular NMR, **23:** 1–12, 2002.
KLUWER/ESCOM

Determination of the glycosidic torsion angles in uniformly ^{13}C-labeled nucleic acids from vicinal coupling constants $^{3}J_{C2/4\text{-}H1'}$ and $^{3}J_{C6/8\text{-}H1'}$

Lukáš Trantírek[a], Richard Štefl[a], James E. Masse[b], Juli Feigon[b,*] & Vladimír Sklenář[a,*]
[a]*National Centre for Biomolecular Research, Faculty of Science, Masaryk University, Kotlářská 2, CZ-611 37 Brno, Czech Republic;* [b]*Department of Chemistry and Biochemistry, 405 Hilgard Avenue, University of California, Los Angeles, CA 90095, U.S.A.*

Received 7 November 2001; Accepted 1 March 2002

Key words: DNA, glycosidic bond, Karplus equation, NMR, quadruplex, scalar coupling

Abstract

A two-dimensional, quantitative J-correlation NMR experiment for precise measurements of the proton-carbon vicinal coupling constants $^{3}J_{C2/4\text{-}H1'}$ and $^{3}J_{C6/8\text{-}H1'}$ in uniformly ^{13}C-labeled nucleic acids is presented. To reduce loss of signal due to ^{1}H -^{13}C dipole-dipole relaxation, a multiple-quantum constant time experiment with appropriately incorporated band selective ^{1}H and ^{13}C pulses was applied. The experiment is used to obtain the $^{3}J_{C2/4\text{-}H1'}$ and $^{3}J_{C6/8\text{-}H1'}$ coupling constants in a uniformly ^{13}C, ^{15}N-labeled $[d(G_4T_4G_4)]_2$ quadruplex. The measured values and glycosidic torsion angles in the G-quadruplex, obtained by restrained molecular dynamics with explicit solvent using the previously published restraints, along with selected data from the literature are used to check and modify existing parameters of the Karplus equations. The parameterizations obtained using glycosidic torsion angles derived from the original solution and recently determined X-ray structures are also compared.

Introduction

Determination of the glycosidic bond angle χ, which defines the orientation of the aromatic base with respect to the ribose (RNA) or 2′-deoxyribose (DNA), is of crucial importance in structural studies of nucleic acids. In nucleic acids, the glycosidic bond can adopt both *anti* or *syn* conformations, in which the aromatic protons H6, H5 in pyrimidine and H8 in purine bases point above ($\chi \sim 240°$) or away from ($\chi \sim 60°$) the sugar ring. A number of methods have been developed to determine the glycosidic torsion angle using NMR spectroscopy, including techniques based on chemical shift changes, proton relaxation time measurements (T_1), analysis of small long-range proton scalar couplings, and utilization of the lanthanide-ion probe (for references see Davies et al., 1985). Of these approaches, only the quantitative evaluation of the inter-proton NOEs and the measurement of three-bond $^{3}J_{C2/4\text{-}H1'}$ and $^{3}J_{C6/8\text{-}H1'}$ coupling constants have been widely used (Wijmenga and Buuren, 1998). The inter-proton H1′-H6 (pyrimidines) and H1′-H8 (purines) sugar-to-base NOEs are obvious candidates for estimating the glycosidic torsion values since the distances differ by 1.2 Å in the *anti* and *syn* conformations. Although the H1′-H6/8 distances are basically independent of the sugar pucker, it is usually not possible to determine χ with accuracy higher than $\pm 50°$ (Wijmenga et al., 1993) due to the experimental ambiguity of the NOE distance determination (± 0.2 Å). The other sugar to base NOEs are dependent in part on the conformation of the sugar ring and can only be used to estimate the global range of the glycosidic bond conformation.

In principle, the vicinal carbon-proton scalar couplings $^{3}J_{C2/4\text{-}H1'}$ and $^{3}J_{C6/8\text{-}H1'}$ can be successfully used for quantitative determination of glycosidic torsion angles providing the correct Karplus relationship between the scalar couplings and the glycosidic torsion is known. Two parameterizations of the Karplus-

*To whom correspondence should be addressed. E-mails: sklenar@chemi.muni.cz; feigon@mbi.ucla.edu

type relationship have been reported to date (Davies et al., 1985; Ippel et al., 1996). However, both depend on data that might have influenced assessment of the Karplus equation parameters (*vide infra*).

So far, only a few methods have been proposed to measure the values of $^3J_{C2/4\text{-}H1'}$ and $^3J_{C8/6\text{-}H1'}$ in DNA and RNA oligonucleotides. Zhu et al. (1994) used the refocused HMBC experiment to extract the scalar couplings in unlabeled DNA quadruplex d(GGTCGG). Schwalbe et al. (1994) and Zimmer et al. (1996) applied a refocused HMBC for the measurements on ^{13}C-labeled oligonucleotides. In general, the HMBC approach suffers from several drawbacks. In both cases, the direct correlation of H1′ protons with base carbons C2/4 and C6/8 (Cb in general) in the HMBC experiment requires rather long evolution delays matching the values of $1/^3J_{Cb\text{-}H1'}$. In addition, the signal-to-noise ratio of individual correlations depends strongly on the value of the particular $1/^3J_{Cb\text{-}H1'}$ coupling constants. For larger ^{13}C-labeled oligonucleotides the long evolution delays will be prohibitive for observing the desired correlations.

Here we propose an approach based on the concept of 2D quantitative J-correlation (Bax et al., 1994), in which the chemical shifts of the H1′ and C1′ atoms are correlated using a multiple-quantum experiment. Two experiments, where the intensity of cross-peaks is modulated by the presence or absence of the H1′-Cb interactions, are used to extract the values of $^3J_{Cb\text{-}H1'}$. The method is demonstrated on the d($G_4T_4G_4$) oligonucleotide, which forms an extremely stable dimeric quadruplex (Smith and Feigon, 1992). Its structure has been refined by restrained molecular dynamics calculations with the explicit solvent using the previously published restraints (Schultze et al., 1994). The measured couplings together with data extracted from the literature are used to check and modify parameters of the existing Karplus equations. The newly derived Karplus parameters slightly improve the quality of the $^3J_{C6/8\text{-}H1'}$ scalar coupling predictions in *syn* and *anti* regions of purine and pyrimidine nucleotides. The parameters obtained for $^3J_{C2/4\text{-}H1'}$ coupling constants are consistent with previously published data for the *anti* orientation of the glycosidic bond but show different patterns for angular dependence of $^3J_{C4\text{-}H1'}$ in purine nucleotides for the *syn* orientation of the glycosidic torsion.

Materials and methods

Sample preparation and NMR spectroscopy

Uniformly ^{13}C,^{15}N-labeled d($G_4T_4G_4$) was enzymatically synthesized using ^{13}C,^{15}N-labeled dNTPs with Taq polymerase on a DNA template and purified as previously described (Masse et al., 1998). Sample conditions were 1.5 mM in quadruplex (3.0 mM strand concentration) in D_2O, 50 mM NaCl, pH 7.2 (uncorrected meter reading) in a total volume of 260 µl in a Shigemi NMR tube.

The NMR data were collected on a Bruker Avance 500 MHz spectrometer equipped with the z-gradient-shielded triple resonance ^{1}H/^{13}C/BB probehead. The data were processed on Silicon Graphic computer (O2) with Bruker NMRSuite programs.

Pulse sequence

The pulse sequence used for the measurement is shown in Figure 1. The constant-time multiple-quantum experiment for H1′-C1′ correlation was used in order to suppress the detrimental influence of the dipole-dipole proton-carbon relaxation and maximize the sensitivity of the experiment (Fiala et al., 1998, 2000). Refocusing of the proton chemical shift evolution during the constant-time period and decoupling of the scalar interactions of H1′ to other protons is achieved by two band-selective pulses with a frequency offset of 5.6 ppm centered in the middle of the $T/2+t_1/2$ and $T/2-t_1/2$ intervals (for details see the figure caption). Due to the symmetry of the chemical shift evolution during two Δ intervals, only one non-selective 180° proton pulse is applied in order to minimize the influence of pulse imperfections. The scalar interactions C1′-C2′ are suppressed using the constant time evolution matching $T = m \times 1/J(C1',C2')$ with band-selective ^{13}C refocusing pulses acting simultaneously on both C1′ and C2′ carbons. Since J(C1′,C2′) in deoxyribose is $\sim$ 38 Hz, the constant-time evolution period is $T\sim m \times 26$ ms. The three-bond coupling constants $^3J_{C2/4\text{-}H1'}$ and $^3J_{C8/6\text{-}H1'}$ are obtained from the intensity changes of H1′/C1′ correlation cross-peaks in two interleaved experiments, in which the interactions C2/4-H1′ or C6/8-H1′ in two separate sets of experiments are alternately coupled and decoupled. The evolution of the C6/8-H1′ and C4/C2-H1′ scalar interactions is controlled by band-selective ^{13}C inversion pulses positioned either in the middle of the $T/2+t_1/2$ and $T/2-t_1/2$ intervals (coupled inter-

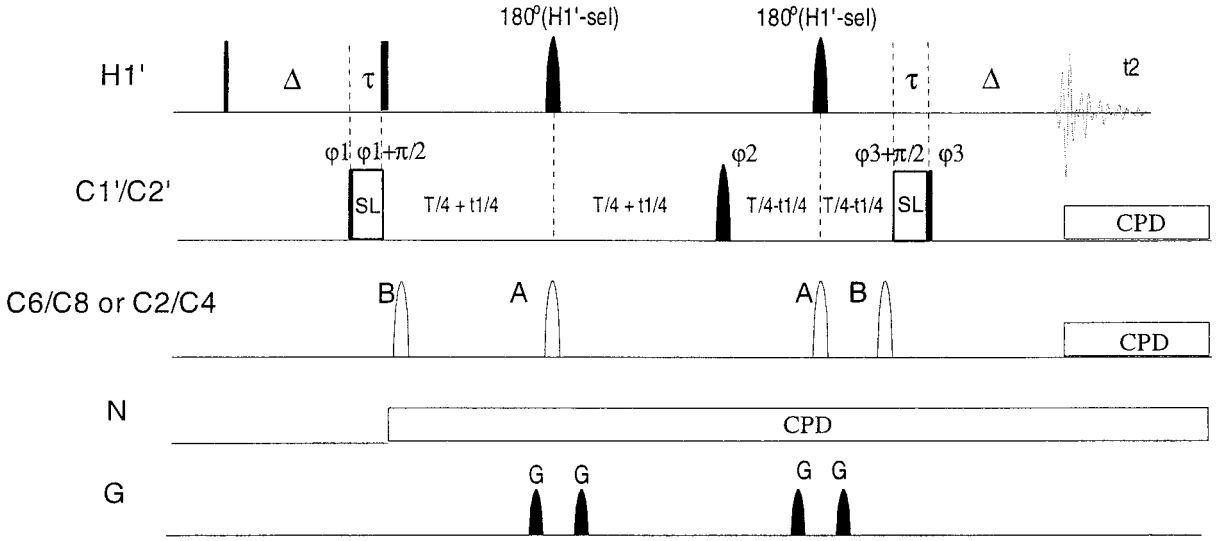

Figure 1. The multiple-quantum experiment for the band-selective H1′-C1′ correlation. The thin and thick bars represent nonselective 90° and 180° pulses, respectively; the SL are optional spin-lock pulses to remove small phase distortions due to the modulation of the selective pulses. Pulses, delays and phase cycles: Δ = 3.2 ms, T = m×26 ms (typically m=2), τ = 1.8 ms. For the actual measurements on $[d(G_4T_4G_4)]_2$ at 500 MHz the band-selective pulses were set as follows: H1′-3 ms 180° Gaussian cascade Q3 centered at 5.6 ppm; ^{13}C-C1′/C2′: 1.5 ms 180° Gaussian cascade Q3 with the carrier at 85 ppm modulated to produce two side-bands with the frequency offsets 0 and −44 ppm; C6/C8 2.0 ms 180° Gaussian cascade Q3 centered at 137 ppm; C2/C4 2.0 ms 180° Gaussian cascade Q3 centered at 155 ppm. Two experiments **A** (coupled H1′-Cb interactions) and **B** (decoupled H1′-Cb interactions) are recorded with the Cb (C6/C8 or C2/C4) pulses positioned as shown in an interleaved manner. For calculations, T = m×26 ms is corrected for the J-evolution during two H1′ band-selective pulses. The correction measured experimentally for the 3 ms Gaussian cascade Q3 was −1.41 ms. Phase cycling: φ_1 = x, −x; φ_2 = 4(x), 4(y), 4(−x), 4(−y); φ_3 = 2(x), 2(−x); receiver: x, −2x, x, −x, 2x, −x. In addition, φ_1 is incremented in States-TPPI manner to achieve quadrature detection in the F_1 dimension. Four identical gradients G (typically 500 μs, 10 G cm^{-1}) are applied.

actions) or at the beginning and at the end of the T interval (decoupled interactions).

Data evaluation

The values of $^3J_{C2/4\text{-}H1'}$ and $^3J_{C6/8\text{-}H1'}$ coupling constants were obtained by relating the integral intensities I_A and I_B of the $^1J_{C1'-H1'}$ peaks in the coupled (A) and decoupled (B) spectra (Figure 1) using the equation:

$$^3J_n = \pi^{-1}T^{-1}\cos^{-1}(R), \quad (1)$$

where n denotes either the C2/4-H1′ or C6/8-H1′ scalar coupling constant, R represents I_A/I_B, and T is the constant time evolution delay.

The standard deviations of coupling constants correspond to uncertainty induced by the presence of spectral noise as discussed by Clore et al. (1998). The error corresponding to the spectral noise is quite small (on average ∼0.16 Hz) since the spectra were collected with very high S/N ratio (> 350). To account for additional errors we have added 0.1 Hz to each value for the data obtained on the $[d(G_4T_4G_4)]_2$ quadruplex. As in other constant time quantitative J-correlation experiments the measured value of J is influenced also by relaxation properties of the passive nuclei, in our case namely by the relaxation of C2/C4 and C6/C8 carbons. As shown by Kuboniwa et al. (1994), the apparent coupling constant $J^r = (J^2\text{-}1/(2\pi T_1)^2)^{1/2}$, where T_1 is the spin-lattice relaxation time of the passive nucleus obtained from the measurements. In $[d(G_4T_4G_4)]_2$ the relaxation times of both C2/C4 and C6/C8 carbons are quite long (>500 ms). The systematic error introduced by the finite length of the spin-lattice relaxation time for J = 3 Hz is less than 0.016 Hz and for J = 5 Hz less than 0.01 Hz.

The standard deviation of the measured J coupling σ_J^2 was evaluated using the error propagation formula (Bevington and Robinson, 1992)

$$\sigma_J^2 \approx \sigma_R^2 \cdot \left(\frac{\partial J}{\partial R}\right)^2, \quad (2)$$

where σ_R^2 is a standard deviation of I_A/I_B, and $J = (\pi T)^{-1}\cos^{-1}(R)$. σ_R^2 was calculated from the relative errors in the determination of attenuated and reference signals:

$$\frac{\sigma_R^2}{R^2} = \frac{\sigma_{Iatt}^2}{I_{att}^2} + \frac{\sigma_{Iref}^2}{I_{ref}^2}. \quad (3)$$

According to the above equations the resulting σ_J^2 depends both on the signal-to-noise ratio and on the magnitude of J.

Model function

The magnitude of a three-bond scalar coupling J depends on the value of the corresponding torsion angle θ. Karplus was the first to quantify this dependence through a series of (real) Fourier coefficients truncated after the third term (Karplus, 1963);

$$J(\theta) = \sum_{m=0}^{2} C_m \cos(m\theta) = C_0 + C_1 \cos(\theta) + C_2 \cos(2\theta). \quad (4)$$

The defined coefficients are physically interpreted as follows: C_0 is the mean J value obtained upon the complete revolution of θ, (C_2-C_1) is the largest deflection in J from the mean, with $2C_1$ being the difference in the scalar coupling between *syn-periplanar* and *anti-periplanar* orientations of the dihedral angle θ.

Equation 4 is more commonly expressed in the following form, which is known as the Karplus equation:

$$^3J(\theta) = A\cos^2\theta + B\cos\theta + C, \quad (5)$$

where the coefficients C_0, C_1 and C_2 from Equation 4 are linked to the coefficients A, B, and C from Equation 5 as follows: $A = 2C_2$, $B = C_1$, and $C = C_0 - C_2$. The torsion angle argument θ for the glycosidic angle χ includes the phase shift and the term accounting for possible distortions in the hybridization geometry of the involved atoms, such that $\theta = \chi + \Delta\chi + \varphi$ where $\Delta\chi$ is the phase shift defined as $\Delta\chi = k\pi/3$ with k = 0, 1,..., 5 to conform with the IUPAC definition of the dihedral angle χ (Markley et al., 1998) and φ is the term accounting for the distortions in hybridization geometry of the involved atoms. For glycosidic torsion, φ contains two contributions ν and ξ which describe the distortions at C1′ and N1/N9 atoms, respectively. The Newman projection for the glycosidic bond along with the definition of ν and ξ is shown in Figure 2.

The non-linear least squares Levenberg–Marquardt fitting procedure, as incorporated in the program Mathematica 3.0 (Wolfram Research, USA), was used to obtain modified parameters of the Karplus equation relating the $^3J_{C2/4\text{-}H1'}$ and $^3J_{C6/8\text{-}H1'}$ scalar coupling constants with values of the glycosidic angle. The fit was directed to minimize the χ^2 merit function given by the sum of squared residuals $\sum_i e_i^2$. Uncertainties in the both measured scalar couplings and glycosidic torsion angle determinations were taken into account during minimization. Each point included in the parameterization was weighted according $(\sigma_J\sigma_\chi)^{-1}$, where σ_J and σ_χ are standard deviations in the given $^3J_{C2/4\text{-}H1'}$ or $^3J_{C6/8\text{-}H1'}$ coupling constant and the corresponding glycosidic torsion angle, respectively.

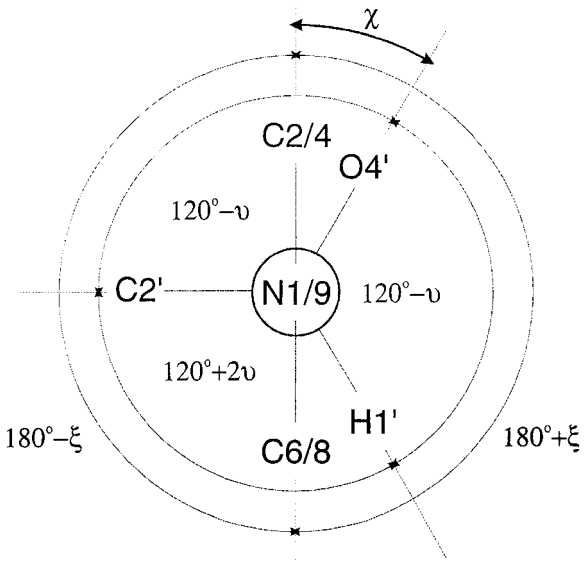

Figure 2. Newman projection of the glycosidic torsion angle viewed along the N1-C1′ and N9-C1′ bond axis for pyrimidines and purines nucleotides, respectively. Dihedral angle contributions ξ = θC6/8-N1/9-C1′-O4′)-180° and ν = θC2/4-N1/9-C1′-H1′)-120° account for possible distortions of ideal planar and tetrahedral bond geometry at N1/9 and C1′ sites, respectively.

Refinement of [d(G$_4$T$_4$G$_4$)]$_2$

We have recalculated the previously determined structure of the [d(G$_4$T$_4$G$_4$)]$_2$ quadruplex (Oxy-1.5) (Schultze et al., 1994) using the original set of restraints and the recently developed methodology of molecular dynamics with the explicit solvent. The restrained MD simulation was performed with the SANDER module of the AMBER 6.0 (Case et al., 1999; Cornell et al., 1995). This force field has been extensively used in studies of quadruplexes (Špačková et al., 1999, 2001; Štefl et al., 2001) as well as other nucleic acids and shows an excellent performance in this respect (Cheatham and Kollman, 2000). It also provides a balanced description of base stacking and hydrogen bonding interactions of nucleic acid bases (Hobza et al., 1997). The refinement was done in a water box containing 4000 H_2O molecules. This ap-

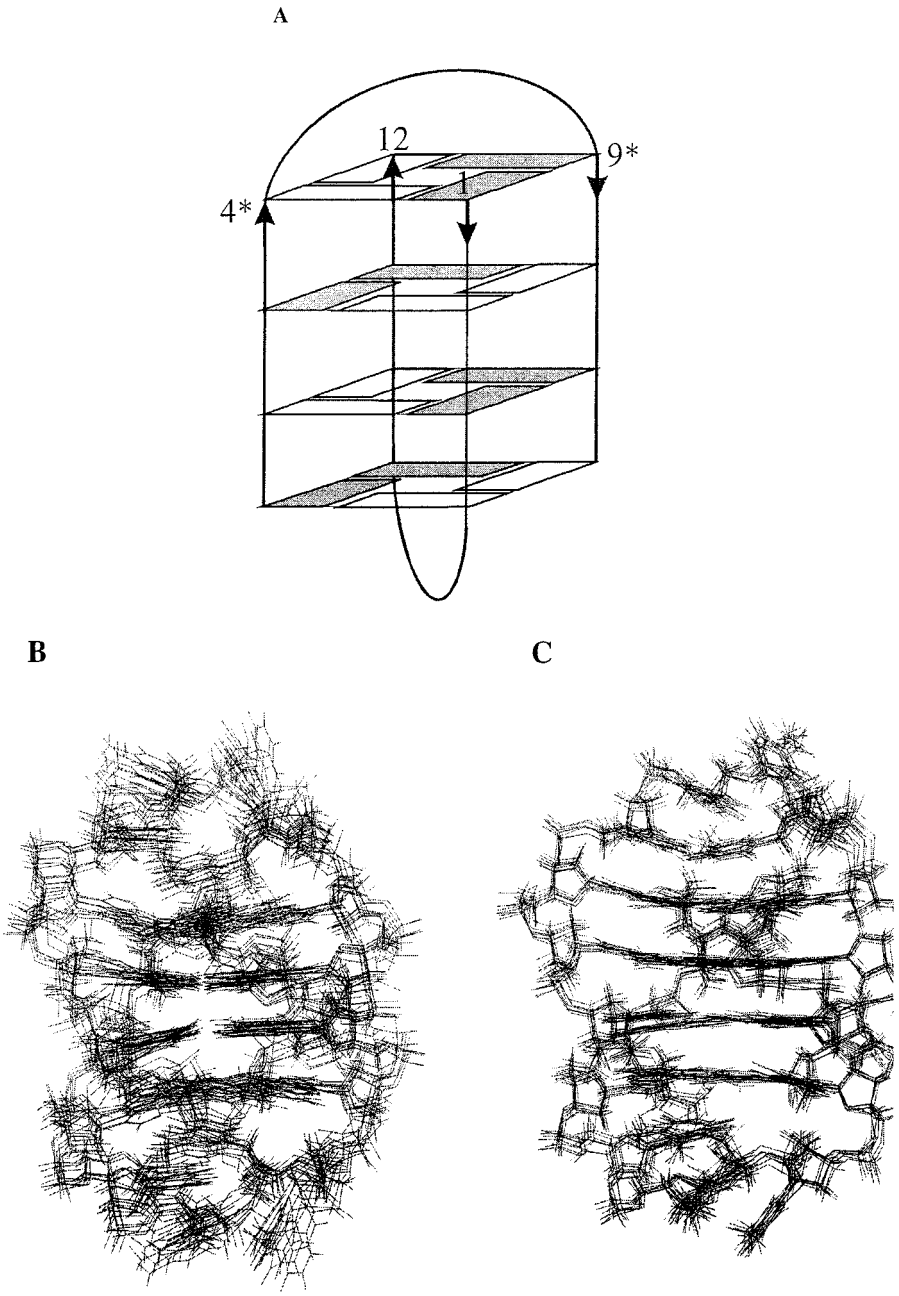

Figure 3. (A) Schematic illustration of the solution structure of $[d(G_4T_4G_4)]_2$. The gray and white boxes are indicative for anti and syn conformation of the glycosidic torsion angles, respectively. (B) Structure ensemble from the original *in-vacuo* refinement (Schultze et al., 1994), (pairwise RMSD 0.95 Å for all heavy atoms). (C) Structure ensemble from the refinement in explicit solvent using the NMR restraints used as in original structure determination (pairwise RMSD 0.55 Å for all heavy atoms).

Table 1. Data points used for re-parameterization of the Karplus equations for $^3J_{C2/4\text{-}H1'}$ and $^3J_{C6/8\text{-}H1'}$

Compound	χ(°)[a]	χ(°)[b,*]		χ(°)[c,*]		$^3J_{C2/4\text{-}H1'}$	(Hz)[$]	$^3J_{C6/8\text{-}H1'}$	(Hz)[$]
Oxy-1.5									
G1	61.4	57.5	(3.5)	56.5	(8.1)	5.60	(0.19)	3.20	(0.16)
G2	254.9	251.4	(8.5)	246.5	(8.6)	2.65	(0.20)	5.01	(0.12)
G3	68.4	65.2	(4.1)	54.9	(8.1)	5.89	(0.17)	3.76	(0.14)
G4	268.6	255.9	(4.0)	260.7	(8.3)	3.12	(0.20)	4.72	(0.12)
T5	251.6	225.4	(5.6)	233.7	(9.4)	3.20	(0.23)	4.05	(0.14)
T6	273.1	235.1	(6.3)	230.3	(10.0)	3.59	(0.22)	4.47	(0.14)
T7	181.7	185.6	(8.8)	171.7	(7.0)	2.06	(0.33)	2.86	(0.20)
T8	249	197.4	(14.7)	225.7	(11.2)	3.12	(0.20)	4.50	(0.13)
G9	64.2	54.7	(5.2)	56.2	(8.1)	5.96	(0.18)	3.49	(0.15)
G10	217.7	241.2	(7.5)	242.6	(7.9)	2.74	(0.24)	4.81	(0.13)
G11	62.5	45.5	(4.1)	53.8	(7.5)	5.67	(0.16)	3.35	(0.14)
G12	264.1	247.3	(6.6)	249.4	(8.2)	2.91	(0.16)	5.10	(0.11)
Nucleotides									
2,5′-anhydro-2′,3′-O-isopropylideneuridine[d]				71.2		#		3.8	(0.2)
2′,6-anhydro-1-(β-D-arabinofuranosyl)-6-hydroxyuracil[d]				70.0		#		3.7	(0.2)
2,2′-anhydro-1-(β-D-arabinofuranosyl)uracil[d]				115		#		0.8	(0.2)
2,2′-anhydro-1-(β-D-arabinofuranosyl)cytosin[d]				115		#		0.6	(0.6)
2,3′-anhydro-1-(β-D-xylofuranosyl)uracil[d]				80		#		3.4	(0.2)
2,5′-anhydro-1-(β-D-ribofuranosyl)uracil[d]				295		0.5	(0.2)	#	
5,6′-anhydro-2′,3′O-isopropylideneuridine[d]				250		2.8	(0.2)	#	
r<pApA>[e]				187		1.2	(0.3)	2.2	(0.4)

[a]Data from X-ray structure (Horvath and Schultz, 2001).
[b]Data from solution NMR structure (Schultze et al., 1994).
[c]The values for glycosidic torsion angle obtained by structure refinement in explicit solvent using NMR restraints published by Schultze et al. (1994).
[d]Selected data from Davies et al. (1985).
[e]Data from Ippel et al. (1996).
*Numbers in brackets represent the dispersion of the glycosidic torsion angle values in the 8(b) and 50(c) energy lowest structures derived from restrained molecular dynamics.
[$]Numbers in brackets represent standard deviations of the measured J couplings calculated according Equation 2 – see Data evaluation.
[#]The J values for these compounds were excluded since the fragments H1′-C1′-N1-C6 or H1′-C1′-N1-C2 were significantly modified at C6 or C2 positions.

proach is particularly suitable for nucleic acids, which have polyelectrolyte character and relative low proton density with a limited number of measurable NMR restraints. Our refinement protocol, consisting of equilibration and molecular dynamic runs, as well as the results of this refinement will be described in detail elsewhere. Only the glycosidic angles extracted from the simulations are presented in Table 1. The angles were obtained from the trajectory using the PTRAJ module of AMBER 6.0.

Quantum chemical calculations

The geometry optimizations of guanine and thymine nucleosides with typical values of glycosidic angles

in the syn and anti conformations and C2′- and C3′-endo sugar puckers were conducted with Gaussian 98 (Gaussian, Inc., USA) using the density functional theory (DFT) method in order to asses the angle strain at C1′, N1 and N9 atoms. These optimizations employed the Becke3P86 hybrid functional and 6-31G** basis set. Quantum chemical calculations were performed on a SGI R10000.

Results and discussion

Glycosidic torsion angles in the G-quadruplex

The structure formed by the DNA oligonucleotide $d(G_4T_4G_4)$, which contains the *Oxytricha* telomere repeat dT_4G_4, forms a symmetrical bimolecular G-quadruplex with four G-quartets and thymine loops which span the diagonal of the end G-quartets (Smith and Feigon, 1992). Guanines are alternately *syn* and *anti* along each strand and all thymines are predominately *anti* (Figure 3A). The $[d(G_4T_4G_4)]_2$ quadruplex has been extensively studied and high resolution structures have been obtained for both Na^+ and K^+ forms using NMR solution data (Schultze et al., 1994; Smith and Feigon, 1992, 1993; Schultze et al., 1999). The identical structural arrangement with diagonally crossing d(TTTT) loops of the Na^+ quadruplex has been recently confirmed by X-ray crystallography at 1.86 Å resolution (Horvath and Schultz, 2001). Since the glycosidic angle conformations alternate between the *syn* and *anti* arrangement along the quadruplex (Figure 3A), this structure represents an ideal model for testing the accuracy of predicted parameters of the Karplus equation. The values of the glycosidic angles found in the originally published NMR structure (Schultze et al., 1994) (Figure 3B), the recent X-ray structure (Horvath and Schultz, 2001), and obtained from the molecular dynamics refinement of the NMR structure reported here (Figure 3C) are given in Table 1. As can be seen, the values in all three structures do not differ significantly. The largest differences are identified in the loop region where contacts with the protein in the crystal can influence the glycosidic torsions at T5, T6 and T8 residues.

Measurement of the $^3J_{C2/4\text{-}H1'}$ and $^3J_{C6/8\text{-}H1'}$ coupling constants

Using the presented pulse sequence we have measured both $^3J_{C2/4\text{-}H1'}$ or $^3J_{C6/8\text{-}H1'}$ scalar couplings in the $[d(G_4T_4G_4)]_2$ quadruplex. The measured couplings are summarized in Table 1. The attempt to fit the data to the existing Karplus equation showed a discrepancy between the experimentally measured coupling constants and the coupling constants predicted based on the known glycosidic angles. As can be seen in Figure 4A, where the Karplus curve defined by the equation 6 has been plotted for $^3J_{C6/8\text{-}H1'}$ (dashed line), the data points measured in the $[d(G_4T_4G_4)]_2$ quadruplex indicate that the current parameterization predicts slightly greater $^3J_{C6/8\text{-}H1'}$ values in both the *syn* and *anti* region. This disagreement, however, is relatively small. The situation is different for the $^3J_{C2/4\text{-}H1'}$ coupling constants (Figure 4B) where in the *syn* region the values of the $^3J_{C2/4\text{-}H1'}$ couplings predicted by the existing parameters are significantly overestimated.

Evaluation of the distortions in the hybridization geometry at C1′, N1 and N9 sites

As a consequence of the cyclic character of the deoxyribose there is an angle strain that influences the hybridization geometry at each atom in the ring. The change in the hybridization geometry should be reflected in the torsion angle argument θ of the Karplus equation (*vide supra*). In order to quantify the effects on the atoms C1′, N1 and N9 we have performed geometry optimizations using the DFT method for a set of guanine and thymine nucleosides with typical values of glycosidic angles in the *syn* (60°) and *anti* (240°) conformation and C2′-endo and C3′-endo sugar puckering. Both terms ν and ξ describing the hybridization geometry changes at C1′ and N1/9 atoms, respectively, are independent of the glycosidic bond conformation. The term ξ has been found to be independent of the orientation of glycosidic bond. The term ν varies slightly with the sugar pucker ($\Delta\nu$(C2′-endo-C3′-endo) = 0.8°). The value of ν for C2′-endo and C3′-endo conformations have been found to be 3.8° and 3.0°, respectively. The difference in ν between 2′-endo and 3′-endo conformations is 0.8° and in practical applications can be safely neglected. Since the deoxyribose rings in $[d(G_4T_4G_4)]_2$ adopt the C2′-endo conformation, we have used $\varphi = -3.8°$ in the torsion angle argument during parameterization (Table 2).

Karplus-type equations for the glycosidic torsion angle

The vicinal carbon-proton coupling constant between nuclei in the base and the sugar ring can potentially

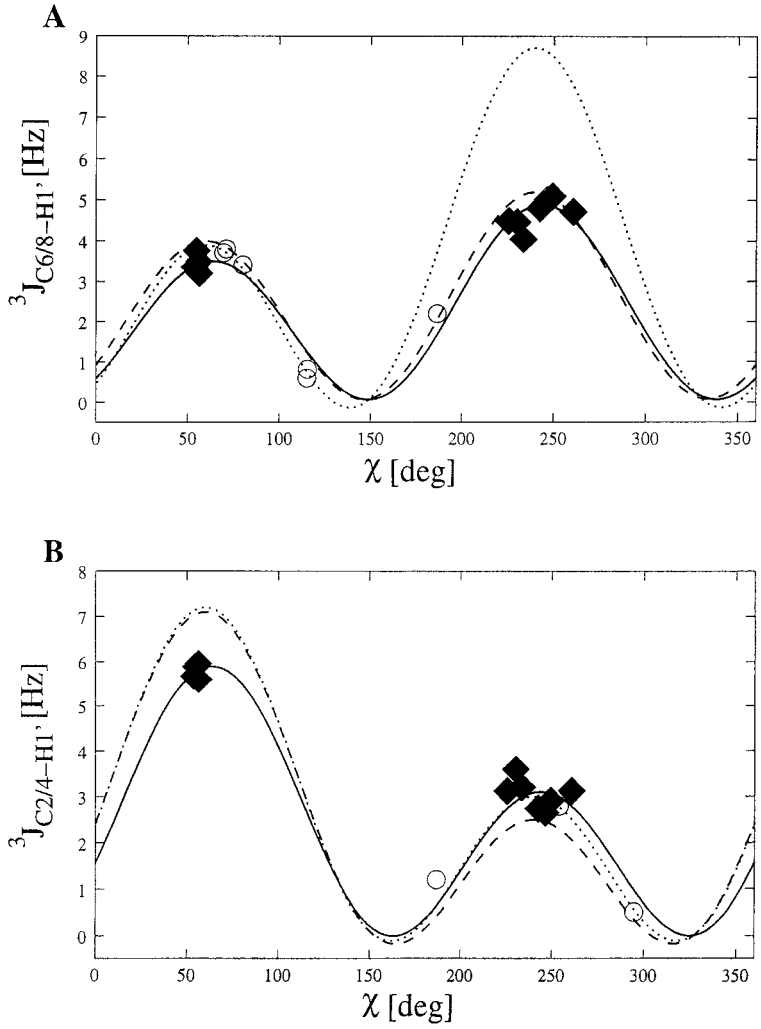

Figure 4. The Karplus curves for $^3J_{C6/8\text{-}H1'}$ (A) and $^3J_{C2/4\text{-}H1'}$ (B). Dotted, dashed and solid lines show the original Davies (Davies et al., 1985), Ippel (Ippel et al., 1996) and the re-parameterized Karplus curve obtained on $[d(G_4T_4G_4)]_2$, respectively. Solid squares represent the data for $[d(G_4T_4G_4)]_2$ and open circles are used for the data points extracted from the literature (Table 1).

be used for the quantitative determination of the glycosidic bond conformation provided the Karplus-type relationship between the coupling constant and torsion angle is known. Lemieux et al. (1972) first pointed out the existence of a Karplus-type relationship between the C2-H1′ and C6-H1′ couplings and the glycosidic torsion angle in uridine nucleosides. Independent support for this hypothesis came from Davies et al. (1985) who used a set of uridine and cytidine cyclonucleosides with known glycosidic bond conformation to propose Karplus-type equations connecting both the $^3J_{C2\text{-}H1'}$ and $^3J_{C6\text{-}H1'}$ couplings with the orientation of the glycosidic bond. Zhu et al. (1994) determined the $^3J_{C4\text{-}H1'}$ and $^3J_{C8\text{-}H1'}$ coupling constants in a DNA G-quadruplex. They used estimated glycosidic torsion angles from the solution structure of a similar G-quadruplex to show that the parameters of the Karplus equation proposed by Davies et al. (1985) for cytidines and uridines could be used for guanidines in the qualitative way as well. Recently, Ippel et al. (1996) demonstrated that the Karplus equations proposed by Davies qualitatively holds for adenosines as well. Using the previously published data and their own results, Ippel et al. (1996) re-parameterized and generalized the Karplus equations for the glycosidic bond conformation of purine and pyrimidine nucleosides and nucleotides in both DNA and RNA:

Table 2. Comparison of the existing parameterizations of the Karplus equations for $^3J_{C2/4\text{-}H1'}$ and $^3J_{C6/8\text{-}H1'}$. D and I denote previously published parameterizations of Davies et al. (1985) and Ippel et al. (1996) , respectively.

J	Ref	Karplus coefficients[a]			Torsion phase increment[b]				RMSD[c]
		A (Hz)	B (Hz)	C (Hz)	k	$\Delta\chi$ (°)	ξ (°)	ν (°)	(Hz)
$^3J_{C2/4\text{-}H1'}$	D	5.0	−2.1	0.1	2	+120	0	0	0.6
$^3J_{C2/4\text{-}H1'}$	I	4.7	2.3	0.1	5	−60	0	0	0.8
$^3J_{C2/4\text{-}H1'}$	NEW	4.4	−1.4	0.1	2	+120	0	−3.8[d]	0.3
$^3J_{C6/8\text{-}H1'}$	D	6.2	−2.4	0.1	5	−60	0	0	1.8
$^3J_{C6/8\text{-}H1'}$	I	4.5	−0.6	0.1	5	−60	0	0	0.4
$^3J_{C6/8\text{-}H1'}$	NEW	4.1	−0.7	0.1	5	−60	0	−3.8[d]	0.3

[a]Coefficients given are for use with the equation $^3J(\theta) = A\cos^2\theta + B\cos\theta + C$ where $\theta = \chi + \Delta\chi + \xi + \nu$.
[b]$\Delta\chi$ is the phase shift defined as $\Delta\chi = k \times \pi/3$ where k = 0, 1, ...,5 to conform with the IUPAC definition of the dihedral angle χ (Markley et al., 1998). Dihedral angle contributions $\xi = \theta$ (C6/8-N1/9-C1′-O4′)-180° and $\nu = \theta$ (C2/4-N1/9-C1′-H1′)-120° account for possible distortions of ideal planar and tetrahedral bond geometry at N1/9 and C1′ sites, respectively.
[c]RMSD root mean squared deviation of the predicted and experimental scalar couplings.
[d]For C2′-endo sugar conformation.

$$^3J_{C6/8\text{-}H1'} = 4.5\cos(\chi - 60) - 0.6\cos(\chi - 60) + 0.1, \quad (6)$$

$$^3J_{C2/4\text{-}H1'} = 4.7\cos(\chi - 60) + 2.3\cos(\chi - 60) + 0.1 \quad (7)$$

These parameterizations, however, were obtained using data sets which were not internally consistent. For 11 points out of 20 used to parameterize Equation 6, the orientations of the glycosidic bond were not known *a priori* and their values were only estimated from similar structures (Ippel et al., 1996; Schmieder et al., 1992; Zhu et al., 1994). In two other model molecules the electronic distribution at the C6 atoms were significantly modified (5′,6-anhydro-2′,3′-O-isopropylideneuridine, and 2′,6-anhydro-1-(β-D-arabinofuranosyl)-6-hydroxyuracil). The situation was similar for the parameterization of the Karplus equation for $^3J_{C2/4\text{-}H1'}$ (Equation 7). In this case, 12 points were used for the parameterization, of which 3 were from estimated glycosidic torsion angles (Ippel et al., 1996; Zhu et al., 1994) and five points were from model molecules with a modified C2 bonding pattern (2,5′-anhydro-2′,3′-O-isopropylideneuridine, 2,5′-anhydro-1-(β-D-ribofuranosyl)uracil, 2,2′-anhydro-1-(β-D-arabinofuranosyl)uracil, 2,2′-anhydro-1-(β-D-arabinofuranosyl) cytosine, 2,3′-anhydro-1-(β-D-xylofuranosyl)uracil). The Ippel parameterizations of the Karplus equations do successfully discriminate between *syn* and *anti* orientations of the glycosidic bond, but are limited in not providing a reliable determination of the torsion angles for purine nucleotides.

Parameterization of the Karplus equation

The $^3J_{C6/8\text{-}H1'}$ and $^3J_{C2/4\text{-}H1'}$ coupling constants and χ angles obtained in this study and the data selected from the literature for structures with known torsion angles and unaffected electronic distributions at C6 and C2 in pyrimidines (Table 1) were used to modify the parameters of the Karplus equation. We have excluded the data points with modified **H1′**-C1′-N1-**C2** and **H1′**-C1′-N1-**C6** fragments since changed electronic distribution might affect the scalar coupling interactions. The J values for T7 were also excluded from the analysis. Residue T7 has a χ value in the range 171°–186° (Table 1), indicating that this residue populates a conformational region very much different from all other residues in the G-quadruplex. Using these χ values, the T7 coupling constants $^3J_{C6/8\text{-}H1'} = 2.3$ Hz and $^3J_{C2/4\text{-}H1'} = 2.0$ Hz do not fit any parameterization of the Karplus equation discussed below. This might be due to conformational averaging over a range of glycosidic torsion angles. Consistent with this, proton resonances of T7 are broader than those of other loop and base resonances (Schultze et al. 1999). It has previously been shown that conformational averaging will affect the parameters of the Karplus equation (Bruschweiler and Case, 1994). Furthermore, the O2 of T7 coordinates a Na^+ located at the top G-quartet in the crystal structure (Horvath and Schultz, 2001) and has been postulated to do so in the solution struc-

ture (Schultze et al., 1999). Therefore, these two data points were excluded from the analysis.

The re-parameterized Karplus curves for $^3J_{C6/8\text{-}H1'}$ and $^3J_{C2/4\text{-}H1'}$ are plotted in Figure 4. Since only a few experimental points are found in regions (0–30°), (100–200°) and (300–360°), the parameter C in Equation 5 was fixed to 0.1 Hz during the fit. This value gives results consistent with the experimentally observed small scalar couplings (< 2Hz) (Zhu et al., 1994; Zimmer et al., 1996) while not significantly influencing the data interpretation in well-defined regions. The obtained and previously published parameters are compared in Table 2.

For $^3J_{C6/8\text{-}H1'}$, the new parameters decrease the RMSD to 0.3 Hz from 0.4 Hz (Ippel) and from 1.8 Hz (Davies). The difference between our parameters and the Ippel parameterization is small. For the Karplus equation describing the dependence of $^3J_{C2/4\text{-}H1'}$ on the angle χ, the Ippel parameterization fits the *anti* region relatively well but predicts substantially greater couplings in the *syn* region than are actually observed. In this context it has to be noted that the data in the *syn* region used here was obtained solely for guanine residues while the Ippel parameterization in the syn region was mainly determined by with the couplings and torsion angles measured on pyrimidine nucleotides. This leaves open the question of whether or not the observed difference is a consequence of the different structural environment of C4 and C2 carbons in purine and pyrimidine bases or if it is due to a less accurate parameterization by Davies and by Ippel. In order to get J values for the *syn* pyrimidines, Davies and Ippel had to use conformationally restricted nucleotide analogs, which could affect the J values relative to standard nucleotides because of a change in electronic environment at C2 and/or additional strain at C1′. Based on the available experimental data, it is not possible to determine whether or not the orientational dependence of $^3J_{C2\text{-}H1'}$ in pyrimidines is the same as of $^3J_{C4\text{-}H1'}$ in purines.

We note that the Ippel parameterization used a phase shift of $-60°$ (Ippel et al., 1996). This value does not alter the fit except for a change in the sign of the parameter B. The phase shift for this coupling constant in our study is set to $+120°$ (for definition see Figure 2). This explains the difference in $\Delta\chi$ shown in Table 2.

For a comparison, the parameters of the Karplus equations for $^3J_{C6/8\text{-}H1'}$ and $^3J_{C2/4\text{-}H1'}$ coupling constants were also obtained using the χ values extracted from the recent X-ray (Horvath and Schultz, 2001) and previously published solution NMR (Schultze et al., 1994) structures. The Karplus coefficients and RMSDs are shown in Table 3. The A, B, and C coefficients are similar and reflect that glycosidic torsion angles in all three structures span the same conformational region. Since the NMR data were obtained in solution, and the structure refined using explicit solvent showed the best convergence, we suggest that Karplus coefficients obtained from this data is the most reliable for practical applications.

Table 3. The parameterizations of the Karplus equations for $^3J_{C2/4\text{-}H1'}$ and $^3J_{C6/8\text{-}H1'}$ using the glycosidic torsion angle values of $[d(G_4T_4G_4)]_2$from the X-ray crystal structure (Horvath and Schultz, 2001), the NMR solution (Schultze et al., 1994), and the structure refinement in explicit solvent using the NMR restraints published by Schultze et al. (1994) in this study

$^3J_{H1'\text{-}C2/4}$	A (Hz)	B (Hz)	C (Hz)	RMSD (Hz)
I	4.5	−1.2	0.1	0.3
II	4.5	−1.4	0.1	0.4
III	4.4	−1.4	0.1	0.3
$^3J_{H1'\text{-}C6/8}$	A (Hz)	B (Hz)	C (Hz)	RMSD (Hz)
I	4.3	−0.8	0.1	0.4
II	4.2	−0.7	0.1	0.4
III	4.1	−0.7	0.1	0.3

The coefficient C was fixed during minimization at 0.1. Torsion angle phase increments for $^3J_{C2/4\text{-}H1'}$ and $^3J_{C6/8\text{-}H1'}$ were fixed at 116.2° and −63.8°, respectively (see Results and Discussion).

To summarize, for $^3J_{C6/8\text{-}H1'}$ the currently used Ippel parameterization and parameters obtained in our study are comparable. Since both parameterizations were derived using the data obtained on pyrimidines and purines, we conclude that the torsion angle dependences of $^3J_{C6\text{-}H1'}$ and $^3J_{C8\text{-}H1'}$ are very similar. In practical applications a single parameterization can be employed. In contrast, for $^3J_{C2\text{-}H1'}$ and $^3J_{C4\text{-}H1'}$ there is a large difference between our parameterization and that of Ippel. This difference may either be (a) due to a difference in the angular dependence of $^3J_{C2\text{-}H1'}$ and $^3J_{C4\text{-}H1'}$ in the *syn* region of pyrimidine and purine residues resulting from the different electronic environment of C2 and C4 carbons or (b) due to a difference in the electronic distributions at the C2 positions from the oxygen bridges of the conformationally modified pyrimidines used for Ippel parameterization.

Caveats in use of the Karplus equation

Despite the improved reliability of the torsion angle prediction, a non-critical use of Karplus equations can still lead to biased assessment of the dihedral angles. The accuracy and precision of the extracted torsion angles strongly depends on the quality Karplus parameters. In order to assess the Karplus coefficients correctly, the experimental points used for parameterization should continuously cover the whole conformational space of a given torsion angle. In practice, however, it is very difficult to satisfy such a requirement. As can be seen from the data used in this study (Table 1, Figure 4), the region of torsion angles around 160° is sparsely populated. Hence, the evaluation of the glycosidic angle from the Karplus equations in this insufficiently defined region must be done with caution.

A general problem in the interpretation of Karplus equation stems from the fact that conformational motion can lead to partial or complete averaging of the vicinal scalar interactions. In our case, the molecular dynamics calculations indicate that there are no large conformational changes on the picosecond timescale for $[d(G_4T_4G_4)]_2$. With the exception of T7, the NMR spectra also do not display features of intermediate or slow conformational exchange on the NMR time-scale.

Summary

A multiple-quantum H1′-C1′ quantitative J-correlation experiment with optimized sensitivity for the measurements of the proton-carbon vicinal coupling constants $^3J_{C2/4\text{-}H1'}$ and $^3J_{C6/8\text{-}H1'}$ in ^{13}C labeled nucleic acids has been designed and successfully tested on the $[d(G_4T_4G_4)]_2$ quadruplex. Since the structure of this DNA quadruplex has been reliably determined both by solution NMR and X-ray crystallography methods, the glycosidic torsion angles and measured $^3J_{C2/4\text{-}H1'}$ and $^3J_{C6/8\text{-}H1'}$ coupling constants were used to obtain a modified set of parameters for the Karplus equation.

Acknowledgements

This work was supported by the Ministry of Education of the Czech Republic, grant LN00A016 to VS and by NIH grant GM48123 and NSF grant NCB-0111060 to JF. We thank Drs Martin Horvath and Steve Schultze for providing the crystal structure coordinates of $[d(G_4T_4G_4)]_2$ prior to publication. The authors are grateful to Radovan Fiala and Lukáš Žídek for critical reading of the manuscript.

References

Bax, A., Vuister, G.W., Grzesiek, S., Delaglio, F., Wang, A.C., Tschudin, R. and Zhu, G. (1994) *Meth. Enzymol.*, **239,** 79–105.

Bevington, P. and Robinson, D.K. (1992) *Data Reduction and Error Analysis for the Physical Sciences*, WCB/McCraw-Hill, U.S.A.

Bruschweiler R. and Case D.A. (1994) *J. Am. Chem. Soc.*, **116**, 11199–11200.

Case, D.A., Pearlman, D.A., Caldwell, J.W., Cheatham III, T.E., Ross, W.S., Simmerling, C.L., Darden, T.A., Merz, K.M., Stanton, R.V., Cheng, A.L. et al. (1999). *AMBER*, 6.0 edn. University of California, San Francisco.

Cheatham, T.E. and Kollman, P.A. (2000) *Annu. Rev. Phys. Chem.*, **51**, 435–471.

Clore G.M., Murphy E., C., Gronenborn A.M. and Bax A. (1998) *J. Magn. Reson.*, **134**, 164–167.

Cornell, W.D., Cieplak, P., Bayly, C.I., Gould, I.R., Merz, K.M., Ferguson, D.M., Spellmeyer, D.C., Fox, T., Caldwell, J.W. and Kollman, P.A. (1995) *J. Am. Chem. Soc.*, **117**, 5179–5197.

Davies, D.B., Rajani, P., MacCoss, M. and Danyluk, S.S. (1985) *Magn. Reson. Chem.*, **23**, 72–77.

Fiala, R., Czernek, J. and Sklenář, V. (2000) *J. Biomol. NMR*, **16**, 291–302.

Fiala, R., Jiang, F. and Sklenář, V. (1998) *J. Biomol. NMR*, **12**, 373–383.

Hobza, P., Kabeláč, M., Šponer, J., Mejzlík, P. and Vondrášek, J. (1997) *J. Comput. Chem.*, **18**, 1136–1150.

Horvath, M.P. and Schultz, S.C. (2001) *J. Mol. Biol.*, **310**, 367–377.

Ippel, J.H., Wijmenga, S.S., de Jong, R., Heus, H.A., Hilbers, C.W., de Vroom, E., van der Marel, G.A. and van Boom, J.H. (1996) *Magn. Reson. Chem.*, **34**, S156–S176.

Karplus, M. (1963) *J. Am. Chem. Soc.*, **85**, 2870–2871.

Kuboniwa, H., Grzesiek, S., Delaglio, F. and Bax, A. (1994) *J. Biomol. NMR*, **4**, 871–878.

Lemieux, R.U., Nagabhushan, T., L. and Paul, B. (1972) *Can. J. Chem.*, **50,** 773–776.

Markley, J.L., Bax, A., Arata, Y., Hilbers, C.W., Kaptein, R., Sykes, B.D., Wright, P.E. and Wuthrich, K. (1998) *J. Mol. Biol.*, **280**, 933–952.

Schmieder, P., Ippel, J., H., van den Elst, H., van der Marel, G., A., van Boom, J., H., Altona, C. and Kessler, H. (1992) *Nucl. Acids Res.*, **20**, 4747–4751.

Schultze, P., Smith, F.W. and Feigon, J. (1994) *Structure*, **2**, 221–233.

Schultze, P., Smith, F.W., Hud, N.V. and Feigon, J. (1999) *Nucl. Acids Res.*, **27**, 3018–3028.

Schwalbe, H., Marino, J.P., King, G.C., Wechselberger, R., Bermel, W. and Griesinger, C. (1994) *J. Biomol. NMR*, **4**, 631–644.

Smith, F.W. and Feigon, J. (1992) *Nature*, **356**, 164–168.

Smith, F.W. and Feigon, J. (1993) *Biochemistry*, **32**, 8682–8692.

Smith, F.W., Lau, F.W. and Feigon, J. (1994) *Proc. Natl. Acad. Sci. USA*, **91**, 10546–10550.

Smith, F.W., Schultze, P. and Feigon, J. (1995) *Structure*, **3**, 997–1008.

Špačková, N., Berger, I. and Šponer, J. (1999) *J. Am. Chem. Soc.*, **121**, 5519–5534.

Špačková, N., Berger, I. and Šponer, J. (2001) *J. Am. Chem. Soc.*, **123**, 3295–3307.

Štefl, R., Špačková, N., Berger, I., Koča, J. and Šponer, J. (2001) *Biophys. J.*, **80**, 455–468.

Wijmenga S.S. and van Buuren B.N.M. (1998) *Prog. Nucl. Magn. Reson. Spectrosc.*, **32**, 287–387

Wijmenga, S.S., Mooren, M.M.W. and Hilbers, C.W. (1993) *NMR of Macromolecules: A Practical Approach*. Oxford University Press, New York.

Zhu, G., Live, D. and Bax, A. (1994) *J. Am. Chem. Soc.*, **116**, 8370–8371.

Zimmer, D.P., Marino, J.P. and Griesinger, C. (1996) *Magn. Reson. Chem.*, **34**, S177–S186.